HHS Public Access

Author manuscript

*Oral Dis*. Author manuscript; available in PMC 2024 March 19.

Published in final edited form as:

*Oral Dis*. 2023 November ; 29(8): 3514–3524. doi:10.1111/odi.14425.

# Phenotypic Variability in *LAMA3*-Associated Amelogenesis Imperfecta

**Shih-Kai Wang**[1,2,*], **Hong Zhang**[3], **Yin-Lin Wang**[1,2], **Figen Seymen**[4], **Mine Koruyucu**[5], **James P. Simmer**[3], **Jan C.-C. Hu**[3]

[1]Department of Dentistry, National Taiwan University School of Dentistry, No.1, Changde St., Taipei City 100, Taiwan

[2]Department of Pediatric Dentistry, National Taiwan University Children's Hospital, No.8, Zhongshan S. Rd., Taipei City 100, Taiwan

[3]Department of Biologic and Materials Sciences, University of Michigan School of Dentistry, 1011 North University, Ann Arbor, MI 48108, USA

[4]Department of Pedodontics, Faculty of Dentistry, Altinbas University, Istanbul, 34147, Turkey

[5]Department of Pedodontics, Faculty of Dentistry, Istanbul University, Istanbul, 34116, Turkey

## Abstract

**Objective—**Amelogenesis imperfecta (AI) is defined as inherited enamel malformations. *LAMA3* (laminin alpha-3) encodes a critical protein component of the basement membrane (laminin-332). Individuals carrying heterozygous *LAMA3* mutations have previously been shown to have localized enamel defects. This study aimed to define clinical phenotypes and to discern the genetic etiology for four AI kindreds.

**Materials and Methods—**Whole exome analyses were conducted to search for sequence variants associated with the disorder, and micro-computed tomography (μCT) to characterize the enamel defects.

**Results—**The predominant enamel phenotype was generalized thin enamel with defective pits and grooves. Horizonal bands of hypoplastic enamel with chalky-white discoloration and enamel hypomineralization were also observed and demonstrated by μCT analyses of affected teeth. Four disease-causing *LAMA3* mutations (NM_198129.4:c.3712dup; c.5891dup; c.7367del; c.9400G>C) were identified. Compound heterozygous *MMP20* mutations (NM_004771.4:c.539A>G; c.692C>T) were also found in one proband with more severe enamel defects, suggesting a mutational synergism on disease phenotypes. Further analyses of the AI-causing mutations suggested that both α3A (short) and α3B (long) isoforms of LAMA3 are essential for enamel formation.

[*]**Corresponding author:** Shih-Kai Wang DDS, PhD, Department of Dentistry, National Taiwan University School of Dentistry, No.1, Changde St., Jhongjheng District, Taipei City 100, Taiwan., shihkaiw@ntu.edu.edu.

Author Contributions

S.-K. Wang, contributed to conception, design, data acquisition, analysis, and interpretation, drafted and critically revised the manuscript; H. Zhang and Y-L. Wang contributed to conception, design, data acquisition, and analysis, and helped draft the original manuscript. F. Seymen, M. Koruyuku, J.P. Simmer, and J.C.-C. Hu contributed to conception, design, data acquisition, and analysis, and critically revised the manuscript. All authors gave their final approval and agreed to be accountable for all aspects of the work.

**Conclusions—**Heterozygous *LAMA3* mutations can cause generalized enamel defects (AI1A) with variable expressivity. Laminin-332 is critical not only for appositional growth but also enamel maturation.

### Keywords

dental enamel; junctional epidermolysis bullosa; laminin; mutation; MMP20; computed tomography

## Introduction

Amelogenesis imperfecta (AI) is a generic diagnosis for genetic disorders characterized by enamel malformations (Hu, Chun, Al Hazzazzi, & Simmer, 2007; Smith et al., 2017). This diagnostic term can be used to describe a solitary dental condition (isolated AI) or syndromes with systemic involvement (syndromic AI). Based upon clinical phenotype (and further subdivided by pattern of inheritance), Witkop classified AI into four main types with 14 subcategories (Witkop, 1988). Type I AI (hypoplastic AI) exhibits reduced enamel thickness with normal radiodensity. Type II (hypomaturation AI) describes a hardness defect (soft enamel) with normal thickness. Type III AI (hypocalcified AI) delineates a severe malformation in which the enamel is extremely soft and subject to rapid post-eruption failure. Type IV AI refers to conditions with somewhat softer and thinner enamel and taurodontism, a dysmorphology of dental roots. Human genetic studies have identified many genes associated with isolated and syndromic AI and demonstrated their essential functions for proper enamel formation (Smith et al., 2017).

Junctional epidermolysis bullosa (JEB) is a group of autosomal recessive conditions featured by blister formation and extensive erosion of the skin and mucus membrane. Biallelic mutations in five genes, *LAMA3* (laminin alpha-3, OMIM*600805), *LAMB3* (laminin beta-3, OMIM*150310), *LAMC2* (laminin gamma-2, OMIM*150292), *COL17A1* (collagen type XVII, OMIM*113811), and *ITGB4* (integrin beta-4, OMIM*147557), have been shown to cause different types of JEB (Has et al., 2020). While *COL17A1* and *ITGB4* encode the transmembrane proteins of hemidesmosomes, *LAMA3, LAMB3*, and *LAMC2* assemble to form laminin-332 (laminin-5) and interact with the membrane proteins to form a basement membrane complex. It has been well documented that all JEB patients exhibit skin fragility and a severe hypoplastic form of AI (syndromic AI) (Wright, Johnson, & Fine, 1993). The affected enamel is thin and full of defective pits and furrows. Also, JEB carriers with heterozygous mutations can have localized enamel defects without skin abnormalities (McGrath et al., 1996). These findings demonstrate that these genes are critical for epithelial cell attachment as well as proper development of dental enamel. Recently, heterozygous *LAMB3* mutations were shown to cause autosomal dominant hypoplastic AI (AI type IA, OMIM#104530) (Kim et al, 2013; Poulter et al., 2014). The enamel phenotype is primarily hypoplastic pits and grooves. On the other hand, while JEB heterozygous carriers of *LAMA3* mutations were reported to have localized enamel defects, descriptions of the enamel phenotypes are limited (Gostyńska et al., 2016; Yuen, Pasmooij, Stellingsma, & Jonkman, 2012) and have yet to determine if heterozygous *LAMA3* mutations can cause more severe enamel malformations.

Here, we characterized four families with autosomal dominant hypoplastic AI and, in each of them, identified a novel *LAMA3* pathogenic mutation. None of the subjects showed JEB related symptoms other than enamel malformations. We further investigate the structural defects of enamel in *LAMA3* mutant teeth from one of the families. This study significantly expands the genotypic and phenotypic spectrums of *LAMA3*-associated AI.

## Materials and Methods

### Subject Recruitment and Mutational Analyses

The human research protocol and consent forms were reviewed and approved by the Institutional Review Boards at the National Taiwan University Hospital and the University of Michigan. All recruited subjects signed written consents after study contents were comprehensively explained, and their questions answered. Detailed history taking and dental examination were performed for phenotyping and constructing family pedigrees. A sample of 2 mL saliva was collected from each participant to obtain genomic DNA for mutational analyses (Chu et al., 2021). All these procedures were specified in our human research protocols and in compliance with the Declaration of Helsinki.

To identify mutations that cause enamel defects, whole exome sequence analyses were performed for all the probands and sometimes their parents and siblings, as described previously (Kim et al., 2019; Y. P. Wang, Lin, Zhong, Simmer, & Wang, 2019). Exome capture was conducted using the SureSelect Human All Exon kits (Agilent Technologies, Inc.), and paired-end sequencing performed using Illumina HiSeq X Ten (for Families 1 and 2)or HiSeq 2500 (for Families 3 and 4) platform (Illumina, Inc.). Potential disease-causing mutations were identified by searching for sequence variants in an in-house list of genes previously associated with enamel formation and/or inherited enamel defects. The sequence variants were evaluated, classified, and interpreted according to the ACMG (American College of Medical Genetics and Genomics) Standards and Guidelines (Richards et al., 2015). Sanger sequencing was used to validate the identified genetic variants and their distribution among recruited family members. Variant frequency, segregation analyses, and polyphen-2 and SIFT analyses helped assess causality. Currently, the NCBI human gene database lists five *LAMA3* cDNA reference sequences (TV1, NM_198129.4; TV2, NM_000227.6; TV3, NM_001127717.4; TV4, NM_001127718.4; TV5, NM_001302996.2) plus eleven TV-X sequences. NG_007853.2 and NM_198129.4 (TV1) and/or NM_000227.6 (TV2) were used to respectively number the gDNA and cDNA positions of identified *LAMA3* sequence variants. For *MMP20* mutations, the NCBI gene (NG_012151.1) and cDNA (NM_004771.4) reference sequences were employed.

### Micro-computed Tomography

To better characterize the enamel defects caused by *LAMA3* mutations, we performed micro-computed tomography (μCT) on three exfoliated primary maxillary left lateral incisors (tooth G) obtained from the Family 1 proband, his twin brother, and an age-matched healthy boy. All samples were scanned over the entire tooth using a SkyScan 1276 In-Vivo Micro-CT System at the Taiwan Mouse Clinic, Academia Sinica. The scanning parameters were set as follows: 18 μm for pixel size, 70 kV and 200 μA for x-ray source, Aluminum

0.5mm + Copper 0.03mm filter, and camera exposure of 332 msec. The data and images were analyzed using software from the SkyScan 3D Software Suite. CTvox was utilized for 3D reconstruction and volume rendering. To calculate tissue volumes, a threshold range of 160-255 was set for enamel, 90-160 for dentin, and 0-50 for dental pulp. HU (Hounsfield Units) density determination and color coding were performed using CTAn (CT-Analyzer) software.

## Results

### Family 1 (NG_007853.2:g.214745dup)

In Family 1 (Figure 1) the proband (II:1) was a 7-year-old boy of Chinese descent who had an identical twin (II:2) (Figure 1a). Clinically, he showed a mixed dentition with normal general tooth morphology (Figure 1b; Figure S1a). However, the enamel of both primary and permanent teeth appeared to be thin with abundant irregular grooves and pitting defects. Several primary teeth had been restored with full-coverage crowns due to these malformations and associated carious lesions. The panoramic radiograph revealed that all unerupted teeth exhibited severe enamel hypoplasia with ragged appearance (Figure 1e). He was otherwise healthy with no history of significant perinatal or infantile illness. Unlike the proband, his twin brother had normal-looking dental enamel clinically and radiographically, although localized pitting defects were observed on his primary teeth (Figure 1c and f; Figure S1b). While the father was reported to have a normal dentition, the mother's teeth showed prominent horizontal bands of hypoplastic enamel with uneven chalky whiteness (Figure 1d; Figure S1c). Sporadic enamel pits were observed on the canines and premolars. Dental attrition was evident, especially on the posterior teeth. Radiographically, the enamel was of normal thickness and radiopacity (Figure 1g). According to the mother, her sister had similar but more severe enamel defects than hers and had undergone extensive dental restorations. The family history and clinical characterization suggested a dominant pattern of disease inheritance with significant phenotypic variability.

Whole exome analyses of the proband, his twin brother, and the mother identified no potential disease-causing mutations in known AI candidate genes except for a heterozygous single nucleotide duplication in *LAMA3* (NM_198129.4:c.5891dup; NM_000227.6:c.1064dup) (ACMG classification: pathogenic, PVS1+PS3+PM2) (Figure 1a). This mutation would introduce a premature termination codon in Exon 47 (NP_937762.2:p.Asp1965*; NP_000218.3:p.Asp356*) and presumably cause the mutant transcript to undergo nonsense mediated decay (NMD) (da Costa, Menezes, & Romão, 2017). It is not documented in the Genome Aggregation Database (gnomAD) (Karczewski et al., 2020), GenomeAsia 100K (Consortium, 2019), or the Taiwan BioBank database (Chen et al., 2016).

### Family 2 (NG_007853.2:g.160520dup)

Family 2 (Figure 2) was a Taiwanese family in which the proband (II:1, age 7) was reportedly the only individual with enamel malformations (Figure 2a). At an early mixed dentition stage, some of his primary teeth showed irregular hypoplastic grooves of enamel, particularly on the facial and occlusal surfaces (Figure 2b; Figure S2a). All erupted

permanent incisors exhibited an abnormal concave labial surface with marked vertical groove defects. Radiographically, while the enamel of most teeth was not particularly thin, the unerupted right maxillary bicuspids showed a “mulberry” appearance of enamel hypoplasia (Figure 2c). In contrast, no apparent enamel malformations were observed in the other 3 family members, although the parents’ teeth showed evident dental attrition (Figure S2b–f). Noticeably, sporadic enamel pits were found on the mother’s teeth, particularly on facial surfaces and cusps. Moreover, a concave defect of enamel hypoplasia was found on her right maxillary central incisor, similar to that of the proband (Figure 2d and e; Figure S2b).

Analysis of proband’s exome identified a heterozygous T-duplication in Exon 30 of *LAMA3* (NM_198129.4:c.3712dup) causing a frameshift and a premature termination codon (NP_937762.2:p.Tyr1238Leufs*3) (ACMG classification: pathogenic, PVS1+PS3+PM2) (Figure 2a). No other pathogenic mutations in known AI-associated genes were detected. Further segregation analysis indicated that this duplication was maternally inherited, as the mother, but not the father or sister, was also heterozygous for the frameshift mutation.

### Family 3 (NG_007853.2:g.229850del)

Family 3 was a consanguineous Turkish family of 5 generations (Figure 3a). The proband (V:4) was a 12-year-old boy who was reportedly the only member having enamel defects in the whole family. Clinically, his permanent teeth looked chalky white without normal enamel translucency (Figure 3b). The tooth surface appeared rough and of many hypoplastic pits. Noticeably, horizontal grooves of defective enamel were also evident on the facial surface of most teeth. Radiographically, the enamel appeared thinner than normal, especially of the anterior teeth (Figure 3e). While being reported to be unaffected, his mother’s (IV:5) teeth showed prominent horizonal bands of hypoplastic enamel and chalky whiteness similar to those observed in the mother of Family 1 (Figure 3c). Pitting defects and surface concavity were also evident on her anterior teeth. The panorex revealed a slightly reduced thickness of dental enamel and decreased contrast between enamel and dentin (Figure 3f). For the other two individuals who were available for dental examination, the father (IV:4) had relatively normal-looking enamel except for prominent attrition and extrinsic staining (Figure S3), and the proband’s older brother (V:3) showed no overt enamel defects but displayed some uneven whiteness on the facial surface of canines and posterior teeth (Figure 3d and g). These characterizations suggested a dominant, rather than recessive, manner of disease inheritance in this consanguineous family, although the phenotypes showed variable expressivity.

Exome analysis of the proband’s DNA identified a single nucleotide deletion in Exon 57 of *LAMA3* (NM_198129.4:c.7367del; NM_000227.6:c.2540del) (ACMG classification: pathogenic, PVS1+PS3+PM2) but no pathogenic sequence variants in other AI candidate genes (Figure 3a). This mutation, which was not documented in any of the genomic databases we scrutinized, causes a frameshift and premature translation termination (NP_937762.2: p.Gly2456Alafs*22; NP_000218.3:p.Gly847Alafs*22), although the mutant transcript will presumably undergo nonsense mediated decay. Segregation analysis of the six recruited family members indicated that the proband (V:4), his mother (IV:5), oldest sister

(V:1), and brother (V:4) were all heterozygous to this mutation, while the father (IV:4) and the second child (V:2) were not.

### Family 4 (NG_007853.2:g.265216G>C)

The proband (III:1) of Family 4 (Figure 4) was a 10-year-old Turkish boy, who inherited enamel malformations from his father (II:3) (Figure 4a). Clinically, both of their dentitions showed hypoplastic enamel with numerous pitting defects that were distributed in a pattern of horizontal bands (Figure 4b–d). In addition, various degrees of hypomineralization were also noticed. While the father's teeth appeared generally chalky white, the proband's exhibited prominent hypomaturation defects. Radiographically, the enamel of proband's teeth was thin and had little contrast with underlying dentin (Figure 4i). The father's teeth were of relatively normal enamel thickness but reduced radiopacity and have undergone extensive attrition and restorative treatments (Figure 4g). In contrast, the teeth of proband's mother (II:2) and younger brother (III:2) appeared generally normal, although the brother's panorex revealed slightly thin enamel of both his primary and permanent teeth (Figure 4e, f, h, and j).

Exome analysis for the proband identified three heterozygous sequence variants in AI candidate genes: two in *MMP20* (NM_004771.4:c.539A>G, NP_004762.2:p.Tyr180Cys; c.692C>T, p.Ala231Val) and one in *LAMA3*, that is variable designated as NM_198129.4:c.9400G>C or NM_000227.6:c.4573G>C (Figure 4a). The *LAMA3* sequence variant is a rare missense mutation (NP_937762.2:p.Asp3134His; NP_000218.3: p.Asp1525His) with an overall MAF of 0.0006 in gnomAD database (ACMG classification: uncertain significance, PM2+PP3+PP4). It was predicted to be probably damaging with a PolyPhen-2 score of 0.988 (Adzhubei et al., 2010). Both *MMP20* missense mutations are not documented in searched databases and predicted probably damaging given PolyPhen-2 scores of 1.000 and 0.999 respectively (ACMG classification of both variants: pathogenic, PS3+PM2+PM3+PP1+PP2+PP3). Further Sanger sequencing and analysis showed that the father carried the *LAMA3* and the c.539A>G *MMP20* mutations, while the mother only had the c.692C>T *MMP20* mutation. The younger brother was heterozygous for the *LAMA3* variant but inherited no *MMP20* mutations. These 2 *MMP20* mutations have never been reported in AI kindreds, bringing the number of known pathogenic MMP20 variants to 24 (Nikolopoulos et al., 2021; S. K. Wang et al., 2020). Phenotypically, it has been demonstrated that biallelic *MMP20* mutations can cause a wide spectrum of enamel malformations, ranging from hypoplastic to hypomaturation defects (S. K. Wang et al., 2013). However, hypoplastic pits and grooves are not a common finding in *MMP20*-associated AI. Therefore, we conclude that the prominent enamel malformations consisting of hypoplastic/hypomaturation enamel with pits and grooves in the proband are likely caused by a synergistic effect from mutations in *LAMA3* and *MMP20*.

### Phenotypic Characterization of LAMA3 Mutant Teeth

Three primary maxillary lateral incisors (tooth letter G), one each from the Family 1 proband, his twin brother, and an unrelated healthy individual, were analyzed using micro-computed tomography (μCT). Three-dimensional reconstructions demonstrated that the proband's tooth ($LAMA3^{Mut}$-1) had numerous deep pits and grooves on all surfaces (Figure

5a). Most of the hypoplastic grooves ran in a vertical direction parallel to the long axis of the tooth. While the twin brother's tooth (*LAMA3*$^{Mut}$-2) appeared grossly comparable to the control (*LAM43*$^{WT}$), its enamel exhibited some surface roughness and localized depressions. Noticeably, unlike a normal incisor, the labial surface of the tooth showed an evident concavity at the middle third. The μCT sections indicated that the pits and grooves of the *LAMA3*$^{Mut}$-1 tooth were confined within the enamel layer, as the dentin appeared unaffected (Figure 5b). Some defects extended to the DEJ with little or no enamel coverage.

Tissue volume analyses demonstrated that the volume percentage of *LAMA3*$^{Mut}$-1 enamel was much smaller (26.42%) than that of *LAMA3*$^{Mut}$-2 (35.40%) and control (35.47%) enamel (Figure 5c). The level of enamel mineralization appeared to be reduced in the *LAMA3* mutant teeth compared to the wild-type (Figure 5b). Although the radiodensities of *LAMA3*$^{Mut}$-1 (95%) and *LAMA3*$^{Mut}$-2 (99%) enamel were only slightly lower than the *LAMA3*$^{WT}$, respectively (Figure 5d), reduced mineralization of its enamel layer close to the DEJ was evident on μCT sections (Figure 5b). However, a slight (3-4%) increase in dentin radiodensity was unexpectedly observed in both *LAMA3* mutant teeth compared to the wild-type. These results suggested that the affected enamel of *LAMA3*-associated AI is not only hypoplastic but also slightly hypomineralized.

## Discussion

To date, there have been two reports demonstrating that carriers of a damaging *LAMA3* mutation exhibit isolated enamel defects (Gostyńska et al., 2016; Yuen et al., 2012). The phenotype is primarily localized rough enamel with hypoplastic pits. However, in this study, we presented 4 families with inherited enamel malformations and demonstrated that heterozygous *LAMA3* mutations can cause not only localized enamel defects but a generalized involvement as isolated AI. Consistent with the enamel malformations reported previously, the defects are primarily hypoplastic (thin) enamel with pits and grooves (furrows). However, some undocumented enamel phenotypes were identified in our families. For example, the mothers of Families 1 and 3 presented with horizontal bands of hypoplastic enamel with chalky-white discolorations. This presentation is similar to the enamel phenotype found in individuals with specific *ENAM* mutations (Kim et al., 2005; Koruyucu et al., 2018; Mårdh et al., 2002). Also, carriers of a *COL17A1* null allele were previously reported to have similar hypoplastic bands of enamel in addition to pitted defects (Murrell et al., 2007). This phenotypic resemblance suggests a molecular interaction among these genes during enamel formation. Furthermore, a hypomaturation or hypomineralization defect was also observed in some of our patients, as the affected enamel showed reduced radiopacity and contrasted less with underlying dentin on radiographs. Our μCT analyses showing decreased enamel radiodensity in *LAMA3* mutant teeth from Family 1 further support this observation. Accordingly, it was previously shown that enamel of JEB patients contains only 60-70% mineral per volume compared to 80-90% in control enamel, indicating a hypomaturation enamel phenotype when laminin-332 is defective (Kirkham et al., 2000). Overall, our characterizations demonstrate a wide phenotypic spectrum of enamel malformations caused by *LAMA3* mutations, including generalized thin enamel, hypoplastic pits and grooves, horizontal bands with chalky whiteness, and enamel hypomaturation. Noticeably, the enamel phenotype can vary significantly among not only individuals

with different mutations but members within a family carrying the same mutation. This phenotypic variability might be explained by mutations in other genes (genetic modifiers). Prasad *et al.* previously reported an individual with heterozygous *COL17A1* and *LAMA3* mutations showing non-syndromic hypoplastic AI with pitting defects and suggested a disease mechanism of digenic inheritance (Prasad et al., 2016). Previously, with an AI family carrying both *ENAM* and *LAMA3* mutations, we also suspected a synergistic effect from these two mutations that caused severe enamel hypoplasia (Zhang et al., 2019). In this study, the father of Family 4 proband carried heterozygous *LAMA3* and *MMP20* mutations and showed pitted enamel with a hypomaturation defect, further demonstrating this phenotypic modification from other mutations. Therefore, it is possible that the phenotypic variability we observed in our families might result from unidentified sequence variants in genes involved in enamel formation. Nevertheless, in Family 1, the severity (expressivity) of enamel defects is extremely different between the proband and his identical twin, suggesting that epigenetic or environmental factors might also significantly contribute to the phenotypic variability in *LAMA3*-associated AI.

It has been well documented that heterozygous *LAMB3* mutations cause pitted autosomal dominant hypoplastic AI (AI1A; OMIM#104530) (Kim et al., 2013; Poulter et al., 2014). The malformed enamel likely results from a dominant negative effect of the mutant protein, since all of the reported mutations are located in the last two exons and lead to generation of a truncated LAMB3 (Smith et al., 2019). Accordingly, enamel defects have never been reported in heterozygous carriers of loss-of-function *LAMB3* or *LAMC2* mutations from JEB families, further suggesting that a single functional allele of these 2 genes is sufficient for proper enamel formation. However, on the contrary, it has been suspected that the localized enamel defects found in carriers of a heterozygous *LAMA3* mutation are caused by haploinsufficiency (Gostyńska et al., 2016; Yuen et al., 2012). All three previously-reported *LAMA3* mutations are apparent loss-of-function variants: c.5315del, p.(Gly1772Aspfs*30); c.7204C>T, p.(Arg2402*) and c.9511+1G>A, p.(?) (Table S1). In this study, we reported 4 novel AI-causing *LAMA3* mutations, including one missense (c.9400G>C) and three indel (c.3712dup; c.5891dup; c.7367del) variants. The 3 indels cause a premature termination codon, and the mutant transcripts presumably undergo nonsense mediated decay. The missense mutation, p.(Asp3134His), substitutes a positively-charged residue, histidine, for a highly conserved, negatively charged, aspartate and would likely cause a loss of function. Also, these pathogenic variants disperse over the gene without mutational homogeneity, which further supports the pathogenesis of haploinsufficiency. These findings suggest that the dose of LAMA3, compared to LAMB3 and LAMC2, has to be tightly regulated during amelogenesis. It has been demonstrated that the LAMA3 monomer pool inside the cell is the smallest among all 3 monomers and used as a regulatory mechanism of heterotrimeric laminin assembly, which corresponds to our notion (Matsui, Wang, Nelson, Bauer, & Hoeffler, 1995). Currently, five LAMA3 protein isoforms are described in the NCBI database. They are generated by different *LAMA3* cDNA transcript variants (TVs) from alternative splicing. While isoforms 1 (NP_937762.2) and 3 (NP_001121189.2) belong to the longer α3B isoforms, 2 (NP_000218.3) and 4 (NP_001121190.2) are categorized as the shorter α3A isoforms, which lack the N-terminal half of α3Bs (Ryan, Tizard, VanDevanter, & Carter, 1994).

The isoform 5 (NP_001289925.1), also known as LaNt alpha31, is a recently-discovered LAMA3 isoform that has not yet been well characterized (Hamill, Langbein, Jones, & McLean, 2009). The functional significance of these isoforms during amelogenesis is largely unknown. The NM_198129.4:c.3712dup mutation, identified in our Family 2, is located at Exon 30 of *LAMA3*, which is not used in TV2 and TV4 for short α3A isoforms, suggesting an indispensable role for long α3B isoforms in enamel formation. Moreover, The NM_198129.4:c.5891dup (NM_000227.6:c.1064dup) mutation, identified from Family 1, resides at Exon 47, which is not included in TV3 and TV4 to generate isoforms 3 and 4, further indicating that these 2 isoforms are not sufficient to serve the full function of LAMA3 during amelogenesis. In other words, isoforms 1 and 2 might play more significant roles in enamel formation. Accordingly, differential expression of various LAMA3 isoforms during enamel formation and their alterations caused by the mutation might underlie the phenotypic variability of *LAMA3*-associated AI.

The hypoplastic enamel defects found in JEB patients and individuals carrying *LAMA3* or *LAMB3* mutations demonstrate that laminin-332 is critical for the appositional growth of enamel formation. Accordingly, laminin-332 subunits have been shown to be highly expressed by secretory ameloblasts, although the basement membrane, more specifically the lamina densa, is degraded at this stage (Sahlberg, Hormia, Airenne, & Thesleff; 1998; Yoshiba et al., 1998). Recently, a molecular model for secretory stage of amelogenesis was proposed (Simmer et al., 2021). A cell attachment apparatus was described for ameloblasts to form and elongate enamel ribbons, where laminin-332 was considered to interact with 2 important enamel matrix proteins, enamelin (ENAM) and ameloblastin (AMBN). Our findings that the enamel phenotypes caused by *LAMA3* mutations are similar to those of *ENAM*-associated AI, including pitting defects and horizontal hypoplastic bands, provide human genetic evidence to support this hypothetical model. Furthermore, the hypomaturation defect we found in our patients also suggests a critical role for laminin-332 during the maturation stage, when a specialized basement membrane is reformed. A *Lamc2* knockout mouse model rescued by human *LAMC2* transgene under the cytokeratin 14 promoter was previously shown to exhibit hypomaturation enamel defects, which supports our findings and confirm that laminin-332 is essential for enamel maturation (Wazen et al., 2016).

In summary, this study demonstrates that both short and long isoforms of LAMA3 are essential for proper enamel formation and argues that, like *LAMB3*, heterozygous *LAMA3* mutations can cause pitted autosomal dominant hypoplastic AI (AI1A).

## Supplementary Material

Refer to Web version on PubMed Central for supplementary material.

## Acknowledgments

We thank the families for participating in the study and the Taiwan Mouse Clinic, Academia Sinica and Taiwan Animal Consortium for the technical support in μCT analyses. This study was supported by Ministry of Science and Technology in Taiwan (MOST) grant, 108-2314-B-002-038-MY3 (SKW); National Taiwan University Hospital (NTUH) grant, 110-N4809 (SKW); and the National Institutes of Health grant R56DE015846 (JCCH). The authors declare no conflict of interest.

## References


Adzhubei IA, Schmidt S, Peshkin L, Ramensky VE,Gerasimova A, Bork P, … Sunyaev SR (2010). A method and server for predicting damaging missense mutations. Nat Methods, 7(4), 248–249. doi:10.1038/nmeth0410-248 [PubMed: 20354512]

Chen CH, Yang JH, Chiang CWK, Hsiung CN, Wu PE, Chang LC, … Shen CY (2016). Population structure of Han Chinese in the modern Taiwanese population based on 10,000 participants in the Taiwan Biobank project. Hum Mol Genet, 25(24), 5321–5331. doi:10.1093/hmg/ddw346 [PubMed: 27798100]

Chu KY, Wang YL, Chou YR, Chen JT, Wang YP, Simmer JP, … Wang SK (2021). Synergistic Mutations of LRP6 and WNT10A in Familial Tooth Agenesis. J Pers Med, 11(11). doi:10.3390/jpm11111217

Consortium GK (2019). The GenomeAsia 100K Project enables genetic discoveries across Asia. Nature, 576(7785), 106–111. doi:10.1038/s41586-019-1793-z [PubMed: 31802016]

da Costa PJ, Menezes J, & Romão L (2017). The role of alternative splicing coupled to nonsense-mediated mRNA decay in human disease. Int J Biochem Cell Biol, 91(Pt B), 168–175. doi:10.1016/j.biocel.2017.07.013 [PubMed: 28743674]

Gostyńska KB, Yan Yuen W, Pasmooij AMG, Stellingsma C, Pas HH, Lemmink H, & Jonkman MF (2016). Carriers with functional null mutations in LAMA3 have localized enamel abnormalities due to haploinsufficiency. Eur J Hum Genet, 25(1), 94–99. doi:10.1038/ejhg.2016.136 [PubMed: 27827380]

Hamill KJ, Langbein L, Jones JC, & McLean WH (2009). Identification of a novel family of laminin N-terminal alternate splice isoforms: structural and functional characterization. J Biol Chem, 284(51), 35588–35596. doi:10.1074/jbc.M109.052811 [PubMed: 19773554]

Has C, Bauer JW, Bodemer C, Bolling MC, Bruckner-Tuderman L, Diem A, … Mellerio JE (2020). Consensus reclassification of inherited epidermolysis bullosa and other disorders with skin fragility. Br J Dermatol, 183(4), 614–627. doi:10.1111/bjd.18921 [PubMed: 32017015]

Hu JC, Chun YH Al Hazzazzi T, & Simmer JP (2007). Enamel formation and amelogenesis imperfecta. Cells Tissues Organs, 186(1), 78–85. doi:10.1159/000102683 [PubMed: 17627121]

Karczewski KJ, Francioli LC, Tiao G, Cummings BB, Alföldi J, Wang Q, … MacArthur DG (2020). The mutational constraint spectrum quantified from variation in 141,456 humans. Nature, 581(7809), 434–443. doi:10.1038/s41586-020-2308-7 [PubMed: 32461654]

Kim JW, Seymen F, Lee KE, Ko J, Yildirim M, Tuna EB, … Hu JC (2013). LAMB3 mutations causing autosomal-dominant amelogenesis imperfecta. J Dent Res, 92(10), 899–904. doi:10.1177/0022034513502054 [PubMed: 23958762]

Kim JW, Seymen F, Lin BP, Kiziltan B, Gencay K, Simmer JP, & Hu JC (2005). ENAM mutations in autosomal-dominant amelogenesis imperfecta. J Dent Res, 84(3), 278–282. doi:10.1177/154405910508400314 [PubMed: 15723871]

Kim JW, Zhang H,Seymen F,Koruyucu M,Hu Y, Kang J, … Hu JC (2019). Mutations in RELT cause autosomal recessive amelogenesis imperfecta. Clin Genet, 95(3), 375–383. doi:10.1111/cge.13487 [PubMed: 30506946]

Kirkham J, Robinson C, Strafford SM, Shore RC, Bonass WA, Brookes SJ, & Wright JT (2000). The chemical composition of tooth enamel in junctional epidermolysis bullosa. Arch Oral Biol, 45(5), 377–386. doi:10.1016/s0003-9969(00)00003-0 [PubMed: 10739859]

Koruyucu M, Kang J, Kim YJ, Seymen F, Kasimoglu Y, Lee ZH, … Kim JW (2018). Hypoplastic AI with Highly Variable Expressivity Caused by ENAM Mutations. J Dent Res, 97(9), 1064–1069. doi:10.1177/0022034518763152 [PubMed: 29554435]

Matsui C, Wang CK, Nelson CF, Bauer EA, & Hoefler WK (1995). The assembly of laminin-5 subunits. J Biol Chem, 270(40), 23496–23503. doi:10.1074/jbc.270.40.23496 [PubMed: 7559513]

McGrath JA, Gatalica B, Li K, Dunnill MG, McMillan JR, Christiano AM, … Uitto J (1996). Compound heterozygosity for a dominant glycine substitution and a recessive internal duplication mutation in the type XVII collagen gene results in junctional epidermolysis bullosa and abnormal dentition. Am J Pathol, 148(6), 1787–1796. [PubMed: 8669466]

Mårdh CK, Bäckman B, Holmgren G, Hu JC, Simmer JP, & Forsman-Semb K (2002). A nonsense mutation in the enamelin gene causes local hypoplastic autosomal dominant amelogenesis imperfecta (AIH2). Hum Mol Genet, 11(9), 1069–1074. doi:10.1093/hmg/11.9.1069 [PubMed: 11978766]

Murrell DF, Pasmooij AM, Pas HH, Marr P, Klingberg S, Pfendner E, … Jonkman MF (2007). Retrospective diagnosis of fatal BP180-deficient non-Herlitz junctional epidermolysis bullosa suggested by immunofluorescence (IF) antigen-mapping of parental carriers bearing enamel defects. J Invest Dermatol, 127(7), 1772–1775. doi:10.1038/sj.jid.5700766 [PubMed: 17344927]

Nikolopoulos G, Smith CEL, Poulter JA, Murillo G, Silva S, Lamb T, … Mighell AJ (2021). Spectrum of pathogenic variants and founder effects in amelogenesis imperfecta associated with MMP20. Hum Mutat, 42(5), 567–576. doi:10.1002/humu.24187 [PubMed: 33600052]

Poulter JA, El-Sayed W, Shore RC, Kirkham J, Inglehearn CF, & Mighell AJ (2014). Whole-exome sequencing, without prior linkage, identifies a mutation in LAMB3 as a cause of dominant hypoplastic amelogenesis imperfecta. Eur J Hum Genet, 22(1), 132–135. doi:10.1038/ejhg.2013.76 [PubMed: 23632796]

Prasad MK, Geoffroy V, Vicaire S, Jost B, Dumas M, Le Gras S, … Bloch-Zupan A (2016). A targeted next-generation sequencing assay for the molecular diagnosis of genetic disorders with orodental involvement. J. Med. Genet, 53(2), 98–110. doi:10.1136/jmedgenet-2015-103302 [PubMed: 26502894]

Richards S, Aziz N, Bale S, Bick D, Das S, Gastier-Foster J, … Committee ALQA (2015). Standards and guidelines for the interpretation of sequence variants: a joint consensus recommendation of the American College of Medical Genetics and Genomics and the Association for Molecular Pathology. Genet Med, 17(5), 405–424. doi:10.1038/gim.2015.30 [PubMed: 25741868]

Ryan MC, Tizard R, VanDevanter DR, & Carter WG (1994). Cloning of the LamA3 gene encoding the alpha 3 chain of the adhesive ligand epiligrin. Expression in wound repair. J Biol Chem, 269(36), 22779–22787. [PubMed: 8077230]

Sahlberg C, Hormia M, Airenne T, & Thesleff I (1998). Laminin gamma2 expression is developmentally regulated during murine tooth morphogenesis and is intense in ameloblasts. J Dent Res, 77(8), 1589–1596. doi:10.1177/00220345980770080601 [PubMed: 9719032]

Simmer JP, Hu JC, Hu Y, Zhang S, Liang T, Wang SK, … Smith CE (2021). A genetic model for the secretory stage of dental enamel formation. J Struct Biol, 213(4), 107805. doi:10.1016/j.jsb.2021.107805 [PubMed: 34715329]

Smith CEL, Poulter JA, Antanaviciute A, Kirkham J, Brookes SJ, Inglehearn CF, & Mighell AJ (2017). Amelogenesis Imperfecta; Genes, Proteins, and Pathways. Front Physiol, 8, 435. doi:10.3389/fphys.2017.00435 [PubMed: 28694781]

Smith CEL, Poulter JA, Brookes SJ, Murillo G, Silva S, Brown CJ, … Mighell AJ (2019). Phenotype and Variant Spectrum in the LAMB3 Form of Amelogenesis Imperfecta. J Dent Res, 98(6), 698–704. doi:10.1177/0022034519835205 [PubMed: 30905256]

Wang SK, Hu Y, Simmer JP, Seymen F, Estrella NM, Pal S, … Hu JC (2013). Novel KLK4 and MMP20 mutations discovered by whole-exome sequencing. J Dent Res, 92(3), 266–271. doi:10.1177/0022034513475626 [PubMed: 23355523]

Wang SK, Zhang H, Chavez MB, Hu Y, Seymen F, Koruyucu M, … Hu JC (2020). Dental malformations associated with biallelic MMP20 mutations. Mol Genet Genomic Med, 8(8), e1307. doi:10.1002/mgg3.1307 [PubMed: 32495503]

Wang YP, Lin HY, Zhong WL, Simmer JP, & Wang SK (2019). Transcriptome analysis of gingival tissues of enamel-renal syndrome. J Periodontal Res, 54(6), 653–661. doi:10.1111/jre.12666 [PubMed: 31131889]

Wazen RM, Viegas-Costa LC, Fouillen A, Moffatt P, Adair-Kirk TL, Senior RM, & Nanci A (2016). Laminin γ2 knockout mice rescued with the human protein exhibit enamel maturation defects. Matrix Biol, 52-54, 207–218. doi:10.1016/j.matbio.2016.03.002 [PubMed: 26956061]

Witkop CJ Jr. (1988). Amelogenesis imperfecta, dentinogenesis imperfecta and dentin dysplasia revisited: problems in classification. J Oral Pathol, 17(9-10), 547–553. [PubMed: 3150442]

Wright JT, Johnson LB, & Fine JD (1993). Development defects of enamel in humans with hereditary epidermolysis bullosa. Arch Oral Biol, 38(11), 945–955. doi:10.1016/0003-9969(93)90107-w [PubMed: 8297258]

Yoshiba N, Yoshiba K, Aberdam D, Meneguzzi G, Perrin-Schmitt F, Stoetzel C, … Lesot H (1998). Expression and localization of laminin-5 subunits in the mouse incisor. Cell Tissue Res, 292(1), 143–149. doi:10.1007/s004410051044 [PubMed: 9506922]

Yuen WY, Pasmooij AM, Stellingsma C, & Jonkman MF (2012). Enamel defects in carriers of a novel LAMA3 mutation underlying epidermolysis bullosa. Acta Derm Venereol, 92(6), 695–696. doi:10.2340/00015555-1341 [PubMed: 22434185]

Zhang H,Hu Y,Seymen F, Koruyucu M,Kasimoglu Y, Wang SK, … Hu JC (2019). ENAM mutations and digenic inheritance. Mol Genet Genomic Med, 7(10), e00928. doi:10.1002/mgg3.928 [PubMed: 31478359]

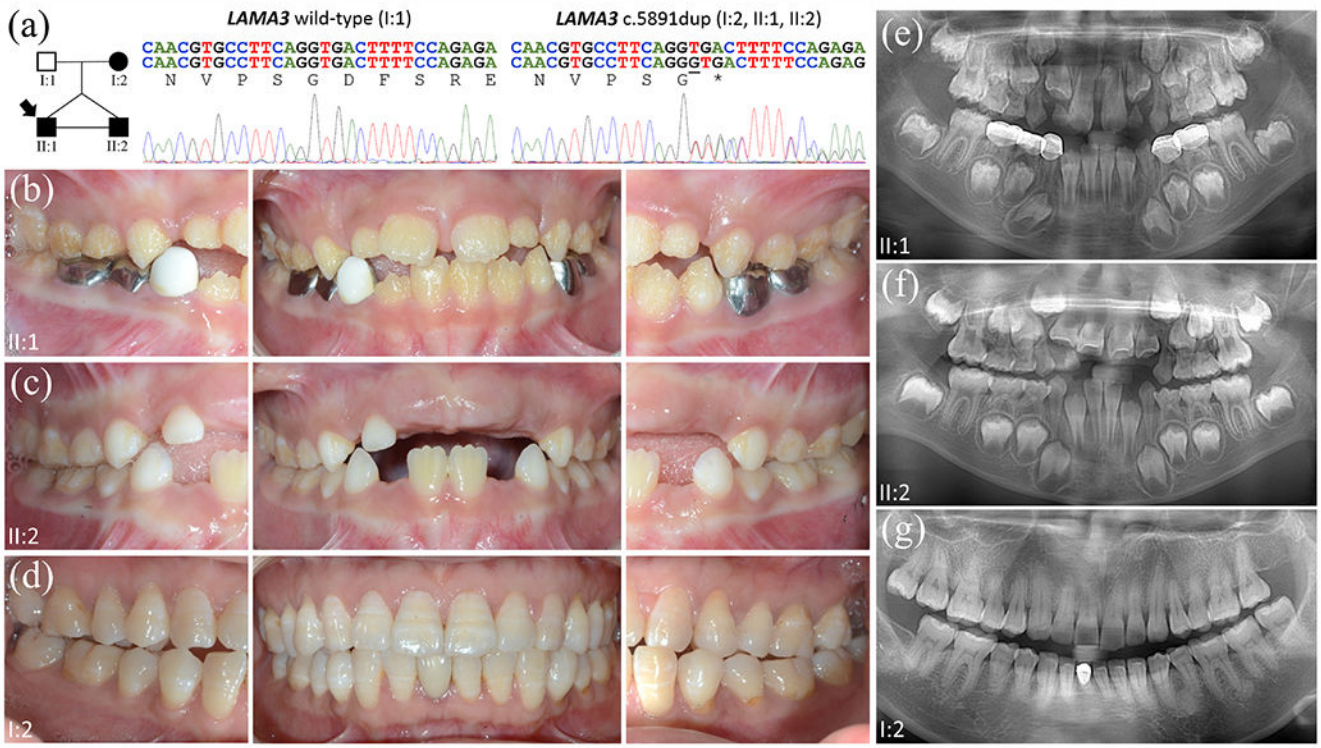


**Figure 1.**

Family 1 with *LAMA3* g.214745dup mutation. (a) The family pedigree suggests a dominant pattern of disease inheritance. The proband has an identical twin brother. The DNA sequencing chromatogram shows a G-duplication (NM_198129.4:c.5891dup) that causes a premature termination codon (NP_937762.2: p.Asp1965*) in one *LAMA3* allele. (b, e) The proband (II:1) at age 7 presented with generalized enamel hypoplasia with irregular pits and grooves. The panorex showed moth-eaten appearance of tooth enamel. (c, f) His twin brother (II:2) had less severe phenotype with some localized enamel pits. (d, g) The mother's (I:2) teeth showed horizontal bands of hypoplastic enamel with chalky-white discolorations. Localized pitted enamel defects and dental attrition were also evident.

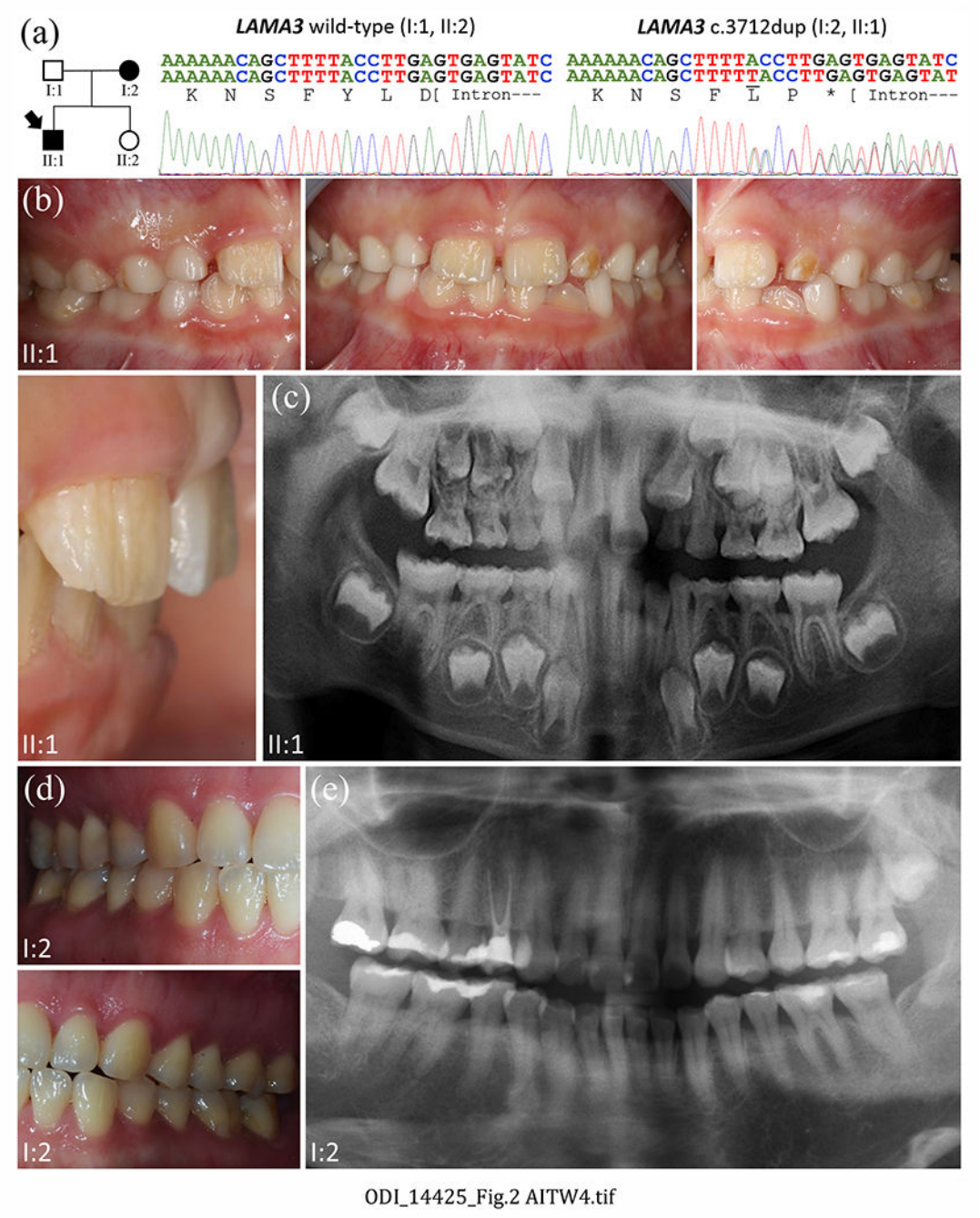


**Figure 2.**

Family 2 with *LAMA3* g.160520dup mutation. (a) The pedigree indicates a nuclear family in which the proband and his mother had enamel malformations. The DNA sequencing chromatogram shows the heterozygous *LAMA3* duplication defect: NM_198129.4:c.3712dup, NP_937762.2:p.Tyr1238Leufs*3 identified in both affected individuals. (b, c) The proband (II:1, age 7) had a mixed dentition showing enamel defects, primarily vertical hypoplastic grooves of facial surface of teeth. The panorex revealed ragged enamel of unerupted tooth numbers 4 and 5. (d, e) The mother (I:2) showed generally

normal-looking enamel except for some pitted defects, particularly on canines and bicuspids. Moderate dental attrition was noticed.

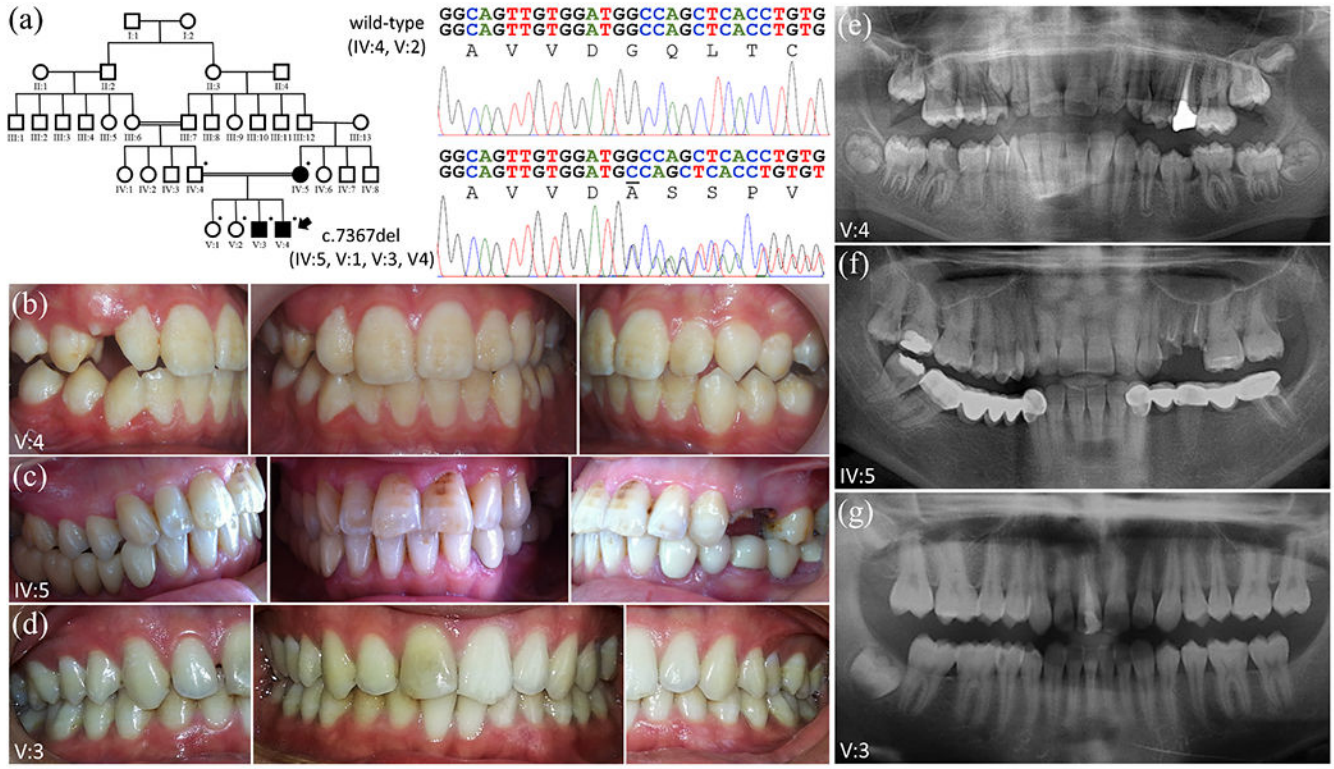


ODI_14425_Fig.3 TKKO.tif

**Figure 3.**

Family 3 with *LAMA3* g.229850del mutation. (a) The pedigree shows a large consanguineous family in which the proband was born of first-cousin marriage. The DNA sequencing chromatogram shows a G-deletion (NM_198129.4:c.7367del) that causes frameshift and a premature termination codon (NP_937762.2: p.Gly2456Alafs*22) in one *LAMA3* allele. (b, e) The proband's (V:4, age 12) teeth exhibited chalky-white appearance with hypoplastic pits and horizontal bands. His panorex showed relatively thin enamel on anterior teeth. (c, f) The mother's (IV:5) teeth showed horizonal bands of hypoplastic enamel with chalky-white discolorations, similar to the phenotype of the mother from Family 1. Pitted defects were also evident. The panoramic radiograph revealed a reduced contrast between enamel and dentin. (d, g) Proband's older brother (V:3) had no apparent enamel defects except for some opaque spots and strips over cervical region of his posterior teeth.

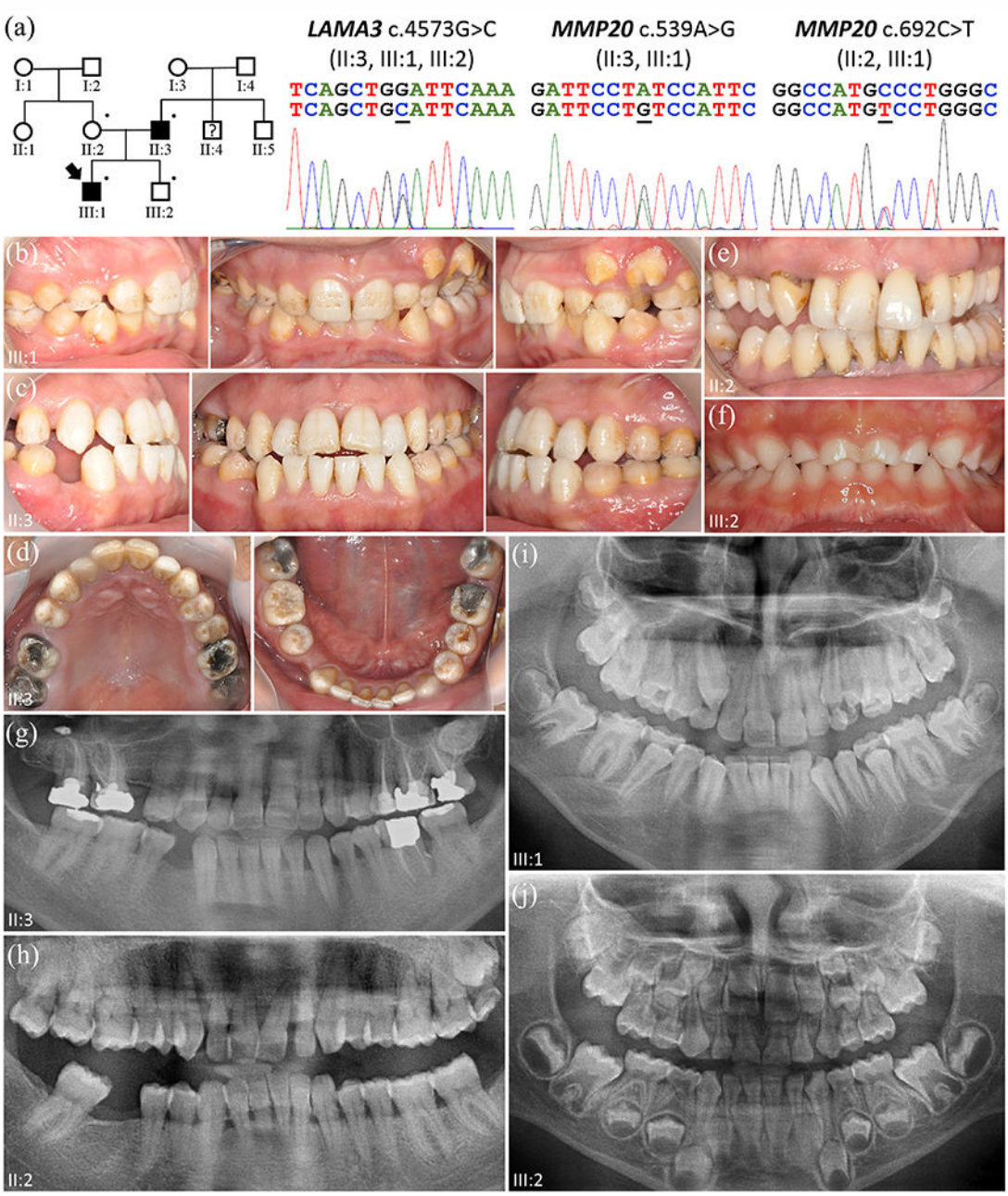


ODI_14425_Fig.4 TKDO.tif

**Figure 4.**

Family 4 with *LAMA3* g.265216G>C and *MMP20* mutations. (a) The pedigree indicates that the proband (III:1) and his father (II:3) are the only 2 individuals with enamel malformations. The DNA sequencing chromatograms from the proband show one *LAMA3* and two *MMP20* heterozygous mutations. While the *LAMA3* variant (NM_198129.4:c.9400G>C) and one *MMP20* mutation (c.539A>G, p.Tyr180Cys) were inherited from his father, the other *MMP20* mutation (c.692C>T, p.Ala231Val) was maternally derived. (b, i) The proband's (age 10) teeth showed both enamel hypoplasia

and hypomaturation with defective pits, which might result from a synergistic effect of *LAMA3* and *MMP20* mutations. The panorex revealed that his enamel was thin and had reduced contrast with underlying dentin. (c, d, g) The father's teeth appeared chalky white and had hypoplastic enamel pits and grooves. His panorex also revealed a reduced radiopacity of tooth enamel. (e, h) The mother (II:2) had no overt enamel defects. (f, j) The proband's brother (III:2) had a primary dentition with normal-looking enamel. The panoramic radiograph showed that the enamel of both his primary and permanent teeth was slightly hypoplastic (thin).

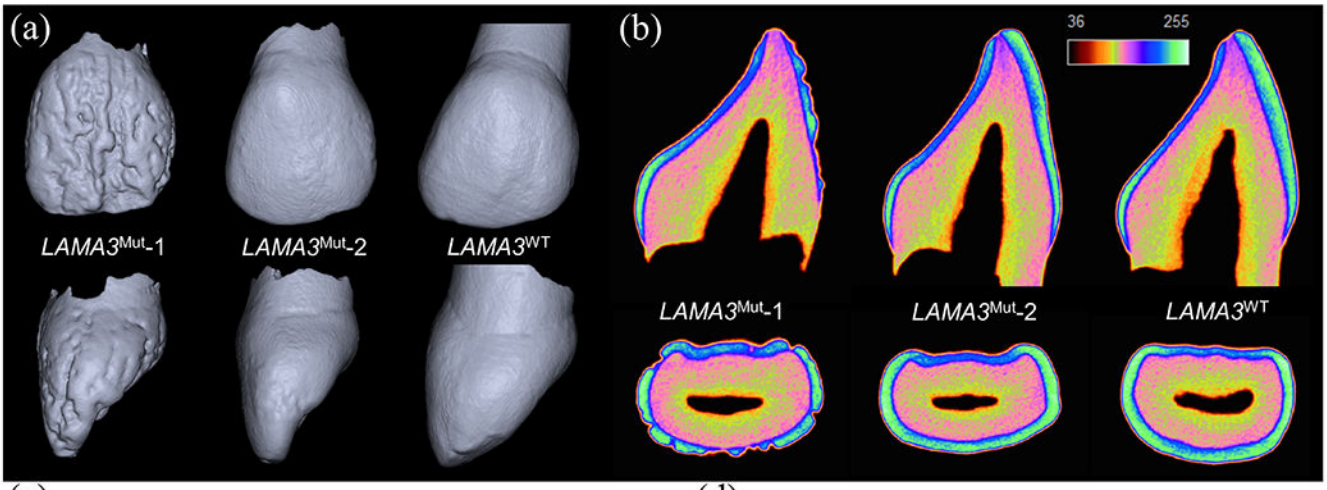


(c)

| Tooth Tissue Volumes ($mm^3$) | | | | | % Enamel Volume | | |
|---|---|---|---|---|---|---|---|
| | *LAMA3*$^{Mut}$-1 | *LAMA3*$^{Mut}$-2 | *LAMA3*$^{WT}$ | | *LAMA3*$^{Mut}$-1 | *LAMA3*$^{Mut}$-2 | *LAMA3*$^{WT}$ |
| Enamel | 12.0718 | 17.5724 | 16.7242 | E/D | 38.8389 | 60.3069 | 61.3016 |
| Dentin | 31.0816 | 29.1383 | 27.2819 | E/(E+D) | 27.9741 | 37.6196 | 38.0043 |
| Pulp | 2.5307 | 2.9284 | 3.1365 | E/(D+P) | 35.9147 | 54.7995 | 54.9806 |
| Total | 45.6841 | 49.6391 | 47.1427 | E/T | 26.4244 | 35.4003 | 35.4758 |

(d)

| Hounsfield Units | | Mean | Std Dev | Std Err | 95%CI (Min) | 95%CI (Max) |
|---|---|---|---|---|---|---|
| Enamel | *LAMA3*$^{Mut}$-1 | 7993.87 | 961.45 | 0.67 | 7992.54 | 7995.21 |
| | *LAMA3*$^{Mut}$-2 | 8299.05 | 912.15 | 0.53 | 8297.99 | 8300.10 |
| | *LAMA3*$^{WT}$ | 8388.83 | 986.34 | 0.58 | 8387.67 | 8390.00 |
| Dentin | *LAMA3*$^{Mut}$-1 | 4378.22 | 1404.43 | 0.58 | 4377.06 | 4379.38 |
| | *LAMA3*$^{Mut}$-2 | 4336.22 | 1465.87 | 0.62 | 4334.98 | 4337.45 |
| | *LAMA3*$^{WT}$ | 4203.79 | 1563.11 | 0.68 | 4202.44 | 4205.14 |

ODI_14425_Fig.5 microCT-v2.tif

**Figure 5.**

Micro-computed tomographic (μCT) analyses of exfoliated primary incisors. Three primary maxillary lateral incisors (tooth letter G) were analyzed, one each from Family 1 proband (LAMA3$^{Mut}$-1), his twin brother (LAMA3$^{Mut}$-2), and a healthy control kid (LAMA3$^{WT}$). (a) Three-dimensional reconstruction of μCT images showing the labial (top) and distal (bottom) views of the teeth. While the proband's tooth showed extremely rough surface with hypoplastic pits and grooves, his twin brother's only had some surface irregularity and depressions. (b) Pseudo-color images of sagittal (top) and transverse (bottom) sections of the teeth. The color coding is based upon the radiodensity of the material. The enamel of *LAMA3* mutant teeth show reduced radiodensity compared to the control. (c) Measurements of tooth tissue volumes and ratios. (d) Radiodensity measurements (in Hounsfield Units) of enamel and dentin.